The Astrophysical Journal Letters, 729:L8 (4pp), 2011 March 1 doi:10.1088/2041-8205/729/1/L8

MAGNETIC KELVIN–HELMHOLTZ INSTABILITY AT THE SUN

Claire Foullon[1], Erwin Verwichte[1], Valery M. Nakariakov[1,2], Katariina Nykyri[3], and Charles J. Farrugia[4]
[1] Centre for Fusion, Space and Astrophysics, Department of Physics, University of Warwick, Coventry CV4 7AL, UK; claire.foullon@warwick.ac.uk
[2] Central Astronomical Observatory of the Russian Academy of Sciences at Pulkovo, 196140 St. Petersburg, Russia
[3] Department of Physical Sciences, Embry-Riddle Aeronautical University, Daytona Beach, FL 32114, USA
[4] Space Science Center and Department of Physics, University of New Hampshire, Durham, NH 03824, USA
Received 2010 December 22; accepted 2011 January 19; published 2011 February 9

ABSTRACT

Flows and instabilities play a major role in the dynamics of magnetized plasmas including the solar corona, magnetospheric and heliospheric boundaries, cometary tails, and astrophysical jets. The nonlinear effects, multi-scale and microphysical interactions inherent to the flow-driven instabilities, are believed to play a role, e.g., in plasma entry across a discontinuity, generation of turbulence, and enhanced drag. However, in order to clarify the efficiency of macroscopic instabilities in these processes, we lack proper knowledge of their overall morphological features. Here we show the first observations of the temporally and spatially resolved evolution of the magnetic Kelvin–Helmholtz instability in the solar corona. Unprecedented high-resolution imaging observations of vortices developing at the surface of a fast coronal mass ejecta are taken by the new *Solar Dynamics Observatory*, validating theories of the nonlinear dynamics involved. The new findings are a cornerstone for developing a unifying theory on flow-driven instabilities in rarefied magnetized plasmas, which is important for understanding the fundamental processes at work in key regions of the Sun–Earth system.

Key words: instabilities – plasmas – solar–terrestrial relations – Sun: corona – Sun: coronal mass ejections (CMEs) – Sun: oscillations

1. INTRODUCTION

Flow-driven instabilities typically arise at flow shear boundaries and are accompanied by energy transfer. A classical example is the Kelvin–Helmholtz (KH) instability, which occurs when two fluids flow at different velocities parallel to a surface of discontinuity with a strong enough shear to overcome the restraining surface tension force. The phenomenon is well understood in fluid and gas dynamics, but is much more challenging in magnetized plasmas typical of space and astrophysical environments, where the three-dimensional topology and various conditions of the rarefied plasma introduce additional constraints and control the characteristics of the resulting disturbances that overcome the magnetic tension force of the curved field lines. At the terrestrial magnetopause, the archetypal natural example of an interface between two plasma regions in sheared flow, a number of instabilities may mediate plasma transfer, mixing, and energization. The KH instability is one that operates on the magnetopause (Hasegawa 1975) with large-scale consequences for its dynamics (e.g., Farrugia et al. 1998; Nykyri & Otto 2001). The instability is believed to be operative in other planetary environments of the solar system (e.g., Amerstorfer et al. 2007; Sundberg et al. 2010, and references therein). Many theories have also explored whether it could occur at fast–slow stream interfaces at the Sun or in the solar wind (Korzhov et al. 1984; Joarder et al. 1997; Suess et al. 2009). Moreover, in flow channels, it is invoked in various solar structures (e.g., Karpen et al. 1993; Ofman et al. 1994; Andries & Goossens 2001; Lapenta et al. 2003; Berger et al. 2010; Ryutova et al. 2010), planetary magnetotails (e.g., McKenzie 1970), cometary tails (e.g., Ershkovich 1980), and astrophysical sources, such as jets in active galactic nuclei and around stellar mass black holes (e.g., Ferrari et al. 1981; Stella & Rosner 1984).

And yet, for an instability so important in space, solar, and astrophysical plasma environments, it has not been possible to find convincing imaging observational evidence of the overall morphological features in the development of this instability. New capabilities for studying the Sun allow us to detect and image KH waves for the first time, in a fast coronal mass ejection (CME) event where the instability develops at the flank of the CME ejecta, and with resolutions unmatched in any other natural plasma laboratory before. These capabilities are provided by the Atmospheric Imaging Assembly (AIA; Lemen et al. 2011) on board the *Solar Dynamics Observatory* (*SDO*), which images the Sun (since end of 2010 March) in 10 white light, ultraviolet and extreme ultraviolet (EUV) bandpasses, covering a wide range of temperatures, at an unprecedented high temporal cadence (up to 10–20 s) and spatial resolution ($0\farcs6$ pixel^{-1}).

2. OBSERVATIONS AND ANALYSIS

The CME event occurred on 2010 November 3, following a C4.9 *GOES* class flare (peaking at 12:15:09 UT from active region NOAA 11121, located near the southeast solar limb). The instability is detected in the highest AIA temperature channel only, centered on the 131Å EUV bandpass at 11 MK. In this temperature range, the ejecta lifting off from the solar surface forms a bubble of enhanced emission against the lower density coronal background, as shown in Figure 1. Along the northern flank of the ejecta, a train of three to four substructures forms a regular pattern in the intensity contrast. Figure 2 shows several snapshots, taken every 12 s, of this northern ejecta flank region, when the substructures are seen to develop. The direction along the ejecta flank is oriented vertically and indicated with distance above the solar surface. The resulting time–distance image allows us to derive the speed of the ejecta front, $V_{\rm ejecta} = 833 \pm 5$ km s^{-1} (projected in the plane of the sky) and to infer that the substructures are coherent, non-dispersive, perturbations that propagate with observational "phase speed," $V_k = 417 \pm 7$ km s^{-1}. The distance between substructures corresponds to a projected wavelength $\lambda = 18 \pm 0.4$ Mm. Thus, the period of these perturbations is 43 ± 2 s.

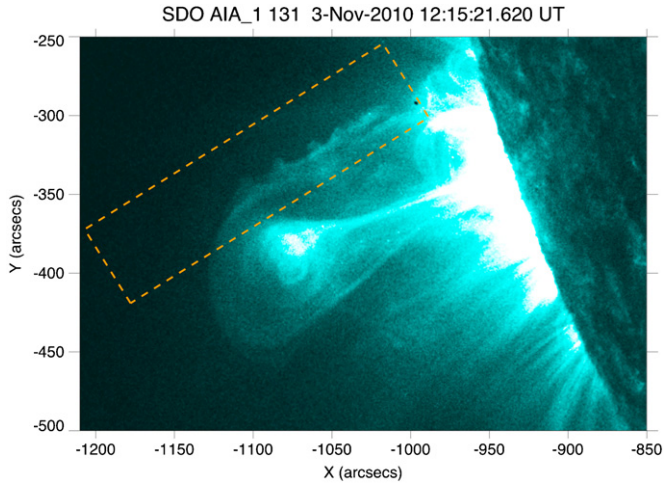

Figure 1. Fast coronal mass ejecta erupting from the Sun, with KH waves detected on its northern flank. The *SDO*/AIA image, shown in solar-centered X (increasing toward west) vs. Y (increasing toward north) coordinates, is taken in the 131 Å channel and centred on the ejecta lifting off the southeast solar limb. With increasing (brighter) intensity levels, it shows the ejecta canopy and within it, a brighter core above a thinner "reconnecting" current sheet. The overlaid rectangular region of interest (ROI) indicates the northern flank region, where substructures, corresponding to the presumed KH waves, are detected against the darker coronal background, and which is used to construct the time–distance image plot in Figure 2.

We interpret these perturbations as KH waves. Considering the convectively unstable surface mode (Mills et al. 2000), perturbations along the boundary surface, while growing, are convected downstream with the corresponding group velocity. The (projected) propagation velocity of the wave envelope or group speed, V_k, is about half the ejecta front speed, $V_{\rm ejecta}$, which may be seen to correspond to limiting cases expected from linear theory (Chandrasekhar 1961; Hasegawa 1975).

The CME flow environment and geometry may be compared to those of the archetypal planetary magnetosphere, with a common onset of the KH instability prescribed by the flow shear directions and the density differences between environments, as sketched in Figure 3 (panels (a) and (b)). While the instability is expected on both sides of the magnetopause for similar magnetic field orientations, some helical configuration of the canopy field can explain here why the phenomena could be observed on one flank of the ejecta only. This helical configuration may be localized (Srivastava et al. 2010) during the finite time (30 ± 6 s) over which the instability is observed to develop, which would be short enough in comparison with the Alfvénic time for the helical twist to be smoothed out. Alternatively, there may be a general helical configuration of the canopy field, but less favorable on the other flank. For instance, the observed asymmetry may be a feature of the azimuthal mode structure of the instability in the twisted field (Zaqarashvili et al. 2010). Additionally, the observed asymmetry may simply result from the preferential line-of-sight viewpoint (similar to the dawn–dusk asymmetry caused by non-zero interplanetary magnetic field (IMF) clock angles (Farrugia et al. 1998; Foullon et al. 2008)). As magnetic field lines reconnect below the ejecta, the flank region of interest appears to rotate around the ejecta axis (starting at time + 48 s in Figure 2), so that the waves are no longer visible in the coronal background contrast but can still be traced as intensity enhancements above the ejecta region. Such rotation of the CME axis has been attributed to kink instability at the onset of the eruption (Foullon et al. 2007), based on similar evidence reported for filament eruptions with axial rotation in the solar corona. This offers a unique opportunity to demonstrate that the instability is indeed localized on this flank region.

A few rolled-up structures are visible in Figures 1 and 2. Much insight has been gained by performing high-resolution numerical simulations, where, e.g., in its nonlinear stage, the instability may set up rolled-up vortices (panel (c) in Figure 3), which entrain magnetic fields of opposing direction (Nykyri & Otto 2004), allowing reconnection to occur as a secondary process and thus, for the magnetopause, allowing solar wind plasma to gain access to the magnetosphere (Nykyri & Otto 2001; Hasegawa et al. 2004). By broadening the

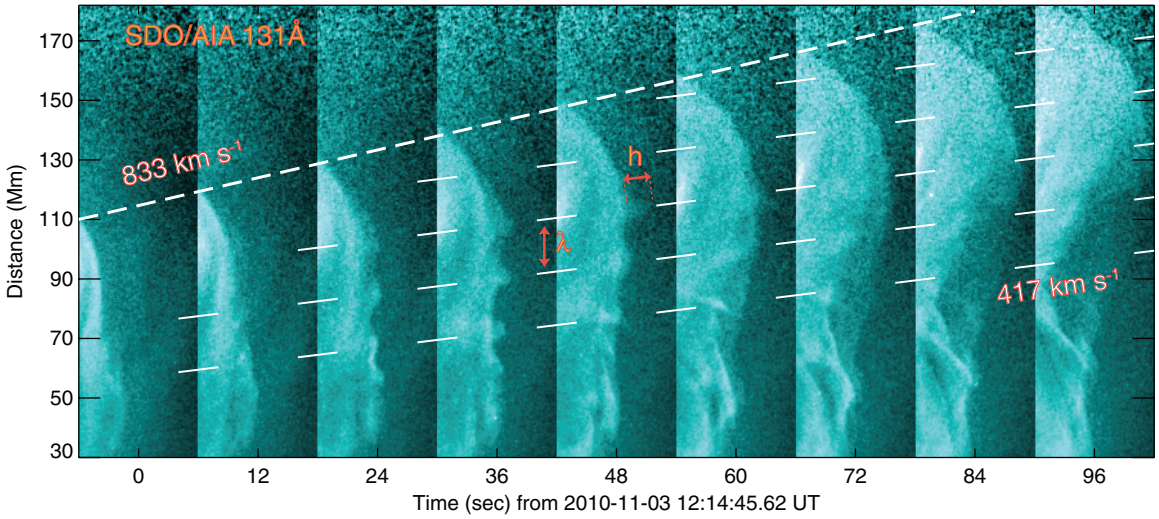

Figure 2. Development of KH waves on the upper ejecta flank region. Snapshots of the ROI overlaid in Figure 1 are taken every 12 s and are directed vertically with increasing distance above the solar surface. To improve the contrast, the intensity is shown relative to a background intensity profile, decreasing with height. This background profile is taken as a running smooth average of the vertical profile obtained from averaging all the ROI images in the horizontal direction. In this time–distance image, the slope of the upper dashed line connecting ejecta front radial positions over time indicates the speed of the ejecta front; the lower slope of the long-dashed lines connecting related substructures indicates an observational "phase speed," V_k, which is about half the former ejecta front speed. The waves are coherent and non-dispersive, with regular separation distances corresponding to wavelength λ, as indicated between two long-dashed lines. One structure is seen to develop to an indicated maximum height h within less than 36 s.

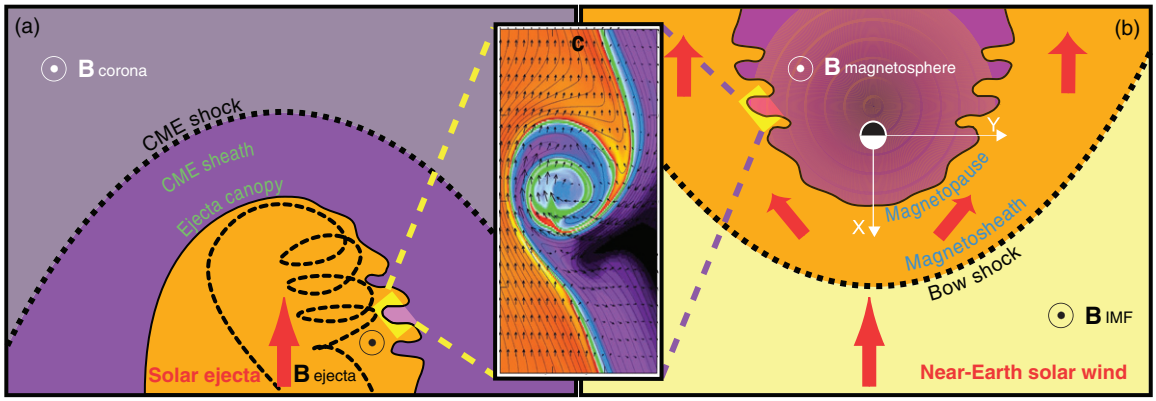

Figure 3. Sketch of comparison of the KH instability conditions in two key regions of the Sun–Earth system, (a) the CME and (b) the magnetosphere, with (c) close-up view on a KH vortex illustrated by numerical simulations (Nykyri et al. 2006). Purple and orange colors indicate low and high plasma density levels. Flow vectors are shown in (c). In the low density regions (purple) being compared: (b) the equatorial cross-section of the magnetosphere is shown with Earth's (almost) dipolar magnetospheric field as viewed from the north; in (a), by analogy, the plane of sky where the waves are detected is shown with the magnetic field canopy of the corona, best represented parallel to the solar surface, pointing in the same direction. In the high density regions (orange) being compared: (b) the best conditions for the KH instability to occur are those of magnetosheath field lines (draped IMF lines around the magnetopause) parallel or anti-parallel to Earth's magnetospheric field, since one can align the wave vector perpendicular to these lines so as to switch off magnetic tensions; in (a), to simplify and facilitate the comparison, the magnetic topological configuration in and around the ejecta is stripped of the presence of current sheet(s) associated with the active region; the ejecta canopy, formed by a magnetic field arcade of loops connected at both ends to the Sun, is overlying a magnetic field flux rope (brightest core in Figure 1). While the instability is expected on both sides of the magnetopause for similar magnetic field orientations, either a localized helical configuration on one flank or a general helical configuration of the canopy field, but less favorable on the other flank, can explain here why the phenomena could be observed on one flank of the ejecta only.

magnetopause boundary layer (Foullon et al. 2008), a layer of mixed magnetospheric and solar wind plasmas just inside and adjacent to the main current sheet, the KH mechanism also contributes to enhance diffusion onto closed field lines (Miura 1984; Phan et al. 1997; Farrugia et al. 2001). However, many of the details of these processes, how they operate, how they "evolve" in time and space, and their importance to the formation of boundary layers and the global dynamics of, e.g., the magnetospheric system, are not fully understood. Using theoretical investigations of the nonlinear dynamics involved by means of magnetohydrodynamics numerical simulations (Miura 1984), the initial total thickness of the velocity shear layer at the fast ejecta interface is inferred to be of the order of $\Delta L = 2.25 \pm 1.5$ Mm (the fastest growing KH modes occur at wavelength approximately 6–12 times ΔL). The *SDO*/AIA images show the formation of a structure reaching size $h \sim 10$ Mm, which developed in 30 ± 6 s (Figure 2), that is with exponential growth rate, $\gamma = 0.05 \pm 0.03$ s^{-1} (using ΔL as the initial size). This result is consistent with predicted linear growth rates (Miura 1984) that are greater than $0.1 \times V_{\rm ejecta}/\Delta L$ for magnetosonic Mach numbers $M_f \geqslant 0.8$, implying a realistic Alfvén speed $V_A \leqslant 918$ km s^{-1} (for the sound speed of $\sim$504 km s^{-1} at 11 MK), and is the first ever direct validation of this theory.

3. DISCUSSION

An important consequence of the presence of KH vortices at CME ejecta (canopy) surfaces is their effect on the total drag force, which affects the CME kinematics and hence its geo-effectiveness (e.g., Foullon et al. 2007). The drag on plasma flows caused by convecting vortex structures is indicated by an anomalous viscosity (Miura 1984). For a transverse flow to magnetic field geometry, the inferred eddy viscosity is of the order of $\nu_{\rm ano} \sim 1.2 \times 10^{-2} \Delta L V_{\rm ejecta}/2 \sim 2 \times 10^{14}$ erg cm^2 s^{-1}, which is an order of magnitude larger than estimates at the magnetopause. With practical implications for space weather forecasting, this effect is relevant to explain differences in drag properties between CMEs (Vršnak et al. 2008; Maloney & Gallagher 2010) considering not only their different speeds and masses, but also their magnetic field topologies. In addition, the asymmetry in drag forces as expected here on the flanks of the ejecta is relevant to explain trajectory deflections or even axial rotations (while it may be noted that the shedding of vortices behind an obstacle can generate quasi-periodic transverse motions (Nakariakov et al. 2009; Gruszecki et al. 2010)).

Also noted here is the occurrence of the instability in the hottest AIA temperature channel. Further detailed examination of the magnetic KH instability will be undertaken in the future. For instance, we note that dissipation, i.e., thermal conduction or viscosity, enhanced in high-temperature plasmas, may have the effect of lowering the instability threshold (Ruderman et al. 1996; Joarder et al. 1997). The range of favorable conditions for the instability to occur and be visible, in combination with the issuing wave characteristics that are observed (period, wavelength, growth rate), means that the instability needs the energy range, time, and spatial resolutions offered by *SDO*/AIA and could not have been observed with previously available instruments. The discovery of the KH instability in the solar corona enables us to deepen our understanding of the three-dimensional geometrical conditions of instability onset, the nonlinear evolution, and its consequences for anomalous viscosity. From a broader point of view, the combined observational and theoretical characterization and the comparison between related solar and terrestrial phenomena allow us to foster a cross-fertilization between the fields and is a promising way to understand the basic plasma physics process at work in flow-driven macroscopic instabilities common to space, solar, and astrophysical plasma environments.

C.F. acknowledges financial support from the UK Science and Technology Facilities Council (STFC) on the CFSA Rolling Grant. AIA data are courtesy of *SDO* (NASA) and the AIA consortium.

Facilities: SDO (AIA)

REFERENCES

Amerstorfer, U. V., Erkaev, N. V., Langmayr, D., & Biernat, H. K. 2007, Planet. Space Sci., 55, 1811
Andries, J., & Goossens, M. 2001, A&A, 368, 1083
Berger, T. E., et al. 2010, ApJ, 716, 1288
Chandrasekhar, S. 1961, Hydrodynamic and Hydromagnetic Stability (International Series of Monographs on Physics; Oxford: Clarendon)
Ershkovich, A. I. 1980, Space Sci. Rev., 25, 3
Farrugia, C. J., Gratton, F. T., & Torbert, R. B. 2001, Space Sci. Rev., 95, 443
Farrugia, C. J., Gratton, F. T., Bender, L., Biernat, H. K., Erkaev, N. V., Quinn, J. M., Torbert, R. B., & Dennisenko, V. 1998, J. Geophys. Res., 103, 6703
Ferrari, A., Trussoni, E., & Zaninetti, L. 1981, MNRAS, 196, 1051
Foullon, C., Farrugia, C. J., Fazakerley, A. N., Owen, C. J., Gratton, F. T., & Torbert, R. B. 2008, J. Geophys. Res., 113, A11203
Foullon, C., et al. 2007, Sol. Phys., 244, 139
Gruszecki, M., Nakariakov, V. M., Van Doorsselaere, T., & Arber, T. D. 2010, Phys. Rev. Lett., 105, 055004
Hasegawa, A. 1975, Plasma Instabilities and Nonlinear Effects (New York: Springer)
Hasegawa, H., Fujimoto, M., Phan, T.-D., Rème, H., Balogh, A., Dunlop, M. W., Hashimoto, C., & TanDokoro, R. 2004, Nature, 430, 755
Joarder, P. S., Nakariakov, V. M., & Roberts, B. 1997, Sol. Phys., 176, 285
Karpen, J. T., Antiochos, S. K., Dahlburg, R. B., & Spicer, D. S. 1993, ApJ, 403, 769
Korzhov, N. P., Mishin, V. V., & Tomozov, V. M. 1984, Planet. Space Sci., 32, 1169
Lapenta, G., Brackbill, J. U., & Daughton, W. S. 2003, Phys. Plasmas, 10, 1577
Lemen, J., et al. 2011, Sol. Phys., submitted
Maloney, S. A., & Gallagher, P. T. 2010, ApJ, 724, L127
McKenzie, J. F. 1970, J. Geophys. Res., 75, 5331
Mills, K. J., Longbottom, A. W., Wright, A. N., & Ruderman, M. S. 2000, J. Geophys. Res., 105, 27685
Miura, A. 1984, J. Geophys. Res., 89, 801
Nakariakov, V. M., Aschwanden, M. J., & Van Doorsselaere, T. 2009, A&A, 502, 661
Nykyri, K., & Otto, A. 2001, Geophys. Res. Lett., 28, 3565
Nykyri, K., & Otto, A. 2004, Ann. Geophys., 22, 935
Nykyri, K., Otto, A., Lavraud, B., Mouikis, C., Kistler, L. M., Balogh, A., & Rème, H. 2006, Ann. Geophys., 24, 2619
Ofman, L., Davila, J. M., & Steinolfson, R. S. 1994, Geophys. Res. Lett., 21, 2259
Phan, T. D., et al. 1997, J. Geophys. Res., 102, 19883
Ruderman, M. S., Verwichte, E., Erdélyi, R., & Goossens, M. 1996, J. Plasma Phys., 56, 285
Ryutova, M., Berger, T., Frank, Z., Tarbell, T., & Title, A. 2010, Sol. Phys., 267, 75
Srivastava, A. K., Zaqarashvili, T. V., Kumar, P., & Khodachenko, M. L. 2010, ApJ, 715, 292
Stella, L., & Rosner, R. 1984, ApJ, 277, 312
Suess, S. T., Ko, Y., von Steiger, R., & Moore, R. L. 2009, J. Geophys. Res., 114, A04103
Sundberg, T., Boardsen, S. A., Slavin, J. A., Blomberg, L. G., & Korth, H. 2010, Planet. Space Sci., 58, 1434
Vršnak, B., Vrbanec, D., & Čalogović, J. 2008, A&A, 490, 811
Zaqarashvili, T. V., Díaz, A. J., Oliver, R., & Ballester, J. L. 2010, A&A, 516, A84